

# Quantum walks on circles in phase space via superconducting circuit quantum electrodynamics

Peng Xue,<sup>1</sup> Barry C. Sanders,<sup>1</sup> Alexandre Blais,<sup>2</sup> and Kevin Lalumière<sup>2</sup>

<sup>1</sup>*Institute for Quantum Information Science, University of Calgary, Alberta, Canada T2N 1N4*

<sup>2</sup>*Département de Physique et Regroupement Québécois sur les Matériaux de Pointe,*

*Université de Sherbrooke, Sherbrooke, Québec, Canada J1K 2R1*

(Received 19 September 2007; revised manuscript received 20 April 2008; published 28 October 2008)

We show how a quantum walk can be implemented in a quantum quincunx created via superconducting circuit quantum electrodynamics (QED) and how interpolation from a quantum to a random walk is implemented by controllable decoherence using a two-resonator system. Direct control over the coin qubit is difficult to achieve in either cavity or circuit QED, but we show that a Hadamard coin flip can be effected via direct driving of the cavity, with the result that the walker jumps between circles in phase space, but still exhibits quantum walk behavior over 15 steps.

DOI: [10.1103/PhysRevA.78.042334](https://doi.org/10.1103/PhysRevA.78.042334)

PACS number(s): 03.67.Ac, 42.50.Pq, 74.50.+r

## I. INTRODUCTION

The quantum walk (QW) is important in physics as a generalization of the ubiquitous random walk (RW), which underpins diffusion and Brownian motion. QWs are important in quantum algorithm research [1] because they exponentially speed up the hitting time in glued tree graphs [2]. Although realization of a QW by a quantum quincunx, analogous to the quincunx (or Galton board) for realizing the RW, has been proposed in ion traps [3] and cavity quantum electrodynamics (QED) [4,5], the former requires cooling of ions to the center-of-mass motional ground state and the latter hitting the atom with pulses that do not drive the cavity at all: these obstacles prevent quantum walks from being realized under foreseeable experimental conditions (a classical optical simulation of a quantum quincunx has been performed [6], but cannot be a proper QW without complementarity [7]).

Here we devise a quantum quincunx that can realize a QW in the laboratory by (i) employing the Jaynes-Cummings model [8] to generalize the Hadamard transformation for coin flipping by directly driving the cavity rather than the atom, (ii) developing a theory of QWs on many circles in phase space (PS) rather than on a single circle as a consequence of generalizing the Hadamard transformation, (iii) optimizing the protocol by having the duration of the generalized Hadamard transformation depend on the time-dependent mean photon number in the cavity (with detailed theory described in Ref. [9]), (iv) implementing in a superconducting circuit QED system [10,11] with a two-level Cooper pair box (CPB) serving as the quantum coin and a coplanar transmission line resonator with a single mode as the quantum walker, (v) introducing a double resonator scheme that can control decoherence while simultaneously enabling strong coupling between the CPB and the microwave field and permitting fast readout, and (vi) using the Holevo standard deviation as a measure of phase spreading and showing that the rate of spreading can be tuned by controllable decoherence to observe the quadratic enhancement of phase spreading for the QW vs RW.

In our scheme the QW is executed with indirect flipping of the coin via directly driving the cavity and allows control-

lable decoherence over circles in PS. Because the walker is directly driven rather than the coin, photon number is no longer conserved and the walker jumps between circles in PS; however, a signature of quantum walking on circles in PS is evident in both the time-dependent phase distribution of the walker and via direct homodyne measurements to obtain the quadrature phase (QP) distribution for the walker. This signature is the scaling of the standard deviation  $\sigma$  (which measures the walker's spreading) that is linear in time  $\propto t$  for the QW and whose power decreases with increasing decoherence until attaining the classical RW scaling  $\propto \sqrt{t}$  for full decoherence. This controllable decoherence is achieved by introducing a second low- $Q$  resonator to obtain fast readout [12].

## II. BACKGROUND

To understand the QW in PS, it is helpful to first understand the RW in PS. The walker is a mode of the resonator and hence is equivalent to a harmonic oscillator, which can be described by its position  $x$  and momentum  $p$ . If the oscillator's energy  $E \sim (\omega^2 x^2 + p^2)/2$  for unit mass and frequency  $\omega$ , then the oscillator follows a periodic circular trajectory of radius  $\sqrt{E}$  in PS with physical oscillatory motion

$$x(t) = \sqrt{E} \cos \omega t. \quad (1)$$

This oscillator can be modified to execute a RW on a circle in PS by periodically applying an impulse that causes it to rotate either clockwise along the circle in PS by angle  $\Delta\theta$  or counter clockwise by the same amount, with the choice of  $\pm\Delta\theta$  strictly random. If  $\Delta\theta = 2\pi/d$ ,  $d \in \mathbb{N}$ , then the walker always remains on a (perhaps rotating) lattice on the circle with angular lattice spacing  $\Delta\theta$ .

We refer to the coordinate in PS  $(x, p)$  as the walker's "location" in PS, and the coin flip randomness that determines clockwise vs counter clockwise angular steps implies that the walker's location is indeterminate and hence described by a distribution  $P(x, p)$ .

In an *ideal* QW on a circle, the walker+coin state is a density operator  $\rho \in \mathcal{B}(\mathcal{H})$  for  $\mathcal{H} = \mathcal{H}_w \otimes \mathcal{H}_c$  (with walker space spanned by  $d-1$  discrete phase states [3,4],

$$\mathcal{H}_w = \text{span}\{|\theta_m = 2m\pi/d\rangle\} \quad (2)$$

and coin space  $\mathcal{H}_c = \text{span}\{|0\rangle, |1\rangle\}$ , where  $\mathcal{B}(\mathcal{H})$  is the Banach space of bounded operators on  $\mathcal{H}$ . The walker's phase distribution on the circle is

$$P_w(\theta) = \langle \theta | \rho_w | \theta \rangle / 2\pi, \quad \rho_w = \text{Tr}_c \rho, \quad (3)$$

with  $d$  equally spaced values of  $\theta = \theta_m$ . However, here the walker is following a circular trajectory in PS, so the QW's Hilbert space is  $\mathcal{H}_w = \text{span}\{|n\rangle; n \in \mathbb{N}\}$ , with  $|n\rangle$  a Fock state ( $\hat{n}$  eigenstate).

Alternatively the generalized position representation  $\{|x\rangle_\varphi\}$  can be used with  $|x\rangle_\varphi$ , an eigenstate of  $\hat{x} \cos \varphi + \hat{p} \sin \varphi$ , for  $\hat{x}, \hat{p}$  the canonical operators satisfying  $[\hat{x}, \hat{p}] = i$  ( $\hbar = 1$ ). The QP distribution is

$$P_\varphi(x) = \langle x | \rho_w | x \rangle_\varphi, \quad (4)$$

with  $\varphi$  the phase of a local oscillator. A convenient correspondence between the classical and quantum PS trajectories of the walker is provided by the Wigner quasiprobability distribution

$$W(x, p) = \int_{-\infty}^{\infty} \frac{dy}{2\pi} e^{ipy} \langle x - y/2 | \rho_w | x + y/2 \rangle, \quad (5)$$

whose marginal distributions are  $P_\varphi(x)$ . Our scheme for realizing the first experimental QW builds on the cavity QED quantum quincunx [4], which alternately applies a coin-flip Hadamard gate

$$H = |+\rangle\langle 0| + |-\rangle\langle 1| \quad (6)$$

for

$$|\pm\rangle = (|0\rangle \pm |1\rangle) / \sqrt{2}, \quad (7)$$

followed by a rotation of the walker's state in PS by  $\pm \Delta \theta$  with the sign depending on the coin state (with  $\hat{n} = \hat{a}^\dagger \hat{a}$  for  $\hat{a} = [\omega \hat{x} + i \hat{p}] / \sqrt{2\omega}$ ):

$$F = \exp(i \hat{n} \hat{\sigma}_z \Delta \theta). \quad (8)$$

The initial state of the walker is a coherent state  $|\alpha\rangle$ :  $\alpha \in \mathbb{R}$  and

$$\langle n | \alpha \equiv \sqrt{\bar{n}_0} \rangle = \sqrt{e^{-\bar{n}_0} \bar{n}_0^n / n!}. \quad (9)$$

Figure 1 depicts PS, including how  $d$  is chosen given an initial walker state  $|\alpha\rangle$  [4]:

$$\bar{n} + \sqrt{\bar{n}} < d < 2\pi \sqrt{\bar{n}}. \quad (10)$$

With this choice, the walker's angular step size is large enough to ensure enough distinguishability to yield a circular QW signature.

The simplicity of this model is rooted in the commutativity of  $(FH)^N$  with  $\hat{n}$ , hence a constant of motion; thus the walker's distance from the PS origin  $\sqrt{\bar{n}}$  is fixed. Unfortunately alternating between  $F$  and  $H$  is not practical in circuit QED. For the QW to be realized and also to have controlled decoherence, a time-dependent driving field for the resonator is needed. As we see below, the sacrifice is that  $[FH, \hat{n}] \neq 0$ , but for realistic circuit QED conditions, the QW on circles is

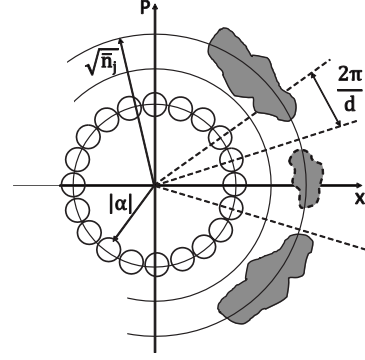


FIG. 1. PS diagram depicting circles of fixed radius  $\sqrt{\bar{n}_j}$  for circle  $j$ . The circle of radius  $|\alpha|$  depicts  $1/e$  contours of the Wigner function for coherent states separated by angular spacing  $2\pi/d$  to make them distinct. A generic Wigner function  $1/e$  contour (boundary of shaded areas) is depicted for circle  $j$  with mean  $\langle \hat{n} \rangle = \bar{n}_j$ . Solid boundaries represent contours around positive peaks, while dashed boundaries are for contours around negative peaks.

(surprisingly) evident provided that the step-by-step  $H$  pulse duration is judiciously chosen.

The goal is to observe the spreading of the QW's phase distribution, and the signature of the QW is that this spread is linear in time: specifically the standard deviation for the phase distribution satisfies  $\sigma \propto t$  for the QW, whereas  $\sigma \propto \sqrt{t}$  for the RW, and the QW can be tuned continuously from the RW by controlling decoherence. As phase is periodic, the usual root-mean-square approach to  $\sigma$  is problematic; instead, we employ the Holevo standard deviation [13]

$$\sigma_H = \sqrt{|\langle e^{i\phi} \rangle|^2 - 1} \quad (11)$$

for

$$\langle e^{i\phi} \rangle = \int_0^{2\pi} d\phi P(\phi) e^{i\phi}, \quad (12)$$

with respect to any phase distribution  $P(\phi)$ , Eq. (3). The Holevo standard deviation is equivalent to the root-mean-square definition for small spreading on the circle, and  $\sigma_H$  naturally quantifies dispersion over all  $\phi \in [0, 2\pi)$  [14]. Thus, for sufficiently short times (less than the time that phase distribution spreads over a significant fraction of the circle in PS), if the relation between phase spreading on the circle with time is a power law, then

$$\ln \sigma_H = \varsigma \ln t + \xi, \quad (13)$$

with  $\varsigma=1$  for the QW and  $\varsigma=1/2$  for the RW.

### III. SUPERCONDUCTING CIRCUIT QUANTUM ELECTRODYNAMICS

The circuit QED Hamiltonian is [10]

$$\hat{H} = \hat{H}_{JC} + \hat{H}_d, \quad \hat{H}_d = \epsilon(t) (\hat{a}^\dagger e^{-i\omega_d t} + \hat{a} e^{i\omega_d t}) \quad (14)$$

for  $\hat{H}_d$  the time-dependent driving field Hamiltonian and

$$\hat{H}_{\text{JC}} = \omega_r \hat{n} + \omega_a \hat{\sigma}_z / 2 + g(\hat{a}^\dagger \hat{\sigma}_- + \hat{a} \hat{\sigma}_+), \quad (15)$$

the Jaynes-Cummings (JC) Hamiltonian, with  $\omega_a$  and  $\omega_r$  the coin and resonator frequencies, respectively, and  $g$  the coupling strength. It is sufficient to let  $\epsilon(t)$  be a square wave, so  $\epsilon$  is a constant ( $\epsilon=0$  when the field is off). In the dispersive regime,

$$|\Delta| = |\omega_a - \omega_r| \gg g, \quad (16)$$

and in a frame rotating at  $\omega_d$  for the qubit and the resonator,  $\hat{H}$  can be replaced by the effective Hamiltonian

$$\hat{H}_{\text{eff}} = \chi \hat{n} \hat{\sigma}_z / -\delta_{\text{da}} \hat{\sigma}_z / 2 - \delta_{\text{dr}} \hat{n} + \Omega_R \hat{\sigma}_x / 2 + \epsilon(\hat{a}^\dagger + \hat{a}), \quad (17)$$

with

$$\delta_{\text{da}} = \omega_d - \omega_a, \quad \delta_{\text{dr}} = \omega_d - \omega_r, \quad (18)$$

$$\Omega_R = 2g\epsilon / \delta_{\text{dr}} \quad (19)$$

the Rabi frequency, and

$$\chi = g^2 / \Delta, \quad (20)$$

the cavity pull of the resonator.

The first term in the above expression effects the coin-induced walker phase shift. The atom transition frequency is ac Stark shifted by  $g^2 \hat{n} \Delta$ . To implement

$$\hat{H} = \exp[i t_H \Omega_R \hat{\sigma}_x / 2] \quad (21)$$

on the coin, we choose

$$\omega_d = 2\bar{n}g^2 / \Delta - 2g\epsilon / \Delta + \omega_a \quad (22)$$

with pulse duration  $t_H = \pi / 2\Omega_R$  and  $\Omega_R$  a function of average photon number:

$$\bar{n}(t) = \text{Tr}(\hat{n} \rho_w). \quad (23)$$

The free evolution

$$\exp(-i \hat{H}_{\text{eff}} t) \quad (24)$$

continues even when the driving field is off ( $\epsilon=0$ ). For time  $\tau$  between  $H$  pulses, the walker steps through an angle

$$\Delta\theta \approx \pm g^2(\tau + t_H) / \Delta. \quad (25)$$

Whereas the ideal QW conserves photon number, Eq. (17) violates this, which we interpret as the walker wandering between circles in PS. Circles have radii  $\sqrt{\bar{n}(t)}$ , and  $\omega_d$  and  $t_H$  are adjusted due to  $\bar{n}(t)$  to ensure that the angular step size  $\Delta\theta$  is constant regardless of how far the walker is from the PS origin. The mean photon number  $\bar{n}(t)$  can be calculated as follows [9]. We begin by solving the Schrödinger equation

$$\frac{d|\varphi\rangle}{dt} = -i \hat{H}_{\text{eff}} |\varphi\rangle \quad (26)$$

from time  $t=0$  to  $t=N(t_H^{(0)} + \tau)$ , for  $N$ , the number of steps,

$$t_H^{(0)} = \pi[\Delta + 2(|\alpha|^2 + 1)\chi - 2g\epsilon / \Delta] / 4g\epsilon \quad (27)$$

and beginning with the initial state

$$|\varphi_0\rangle = (|0\rangle + i|1\rangle)|\alpha\rangle / \sqrt{2}. \quad (28)$$

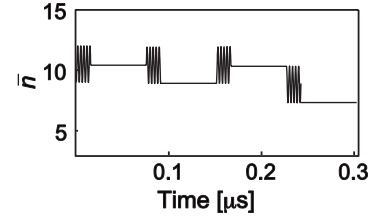


FIG. 2. Average photon number  $\bar{n}$  vs evolution time  $t$  ( $\mu\text{s}$ ) with period  $(t_H^{(0)} + \tau)$ .

Figure 2 plots  $\bar{n}(t)$  for  $\alpha=3$ ,  $d=21$ , and realistic system parameters [15,16]

$$(\omega_a, \omega_r, g, \epsilon) / 2\pi = (7000, 5000, 100, 1000) \text{ MHz}. \quad (29)$$

It is evident in the figure that the mean number oscillates and then settles down during the free evolution, so the walker is concentrated on a circle of squared radius,

$$\bar{n}_j = (t_H^{(0)} + \tau)^{-1} \int_{(j-1)(t_H^{(0)} + \tau)}^{j(t_H^{(0)} + \tau)} \bar{n}(t) dt, \quad (30)$$

at step  $j$ . The corresponding Hadamard pulse duration  $t_H^{(j)}$  for each step  $j$  is

$$t_H^{(j)} = \pi[\Delta + 2(\bar{n}_j + 1)\chi - 2g\epsilon / \Delta] / 4g\epsilon \quad (31)$$

for  $j \in \mathbb{N}$ ,  $\bar{n}_0=9$ , and  $t_H^{(0)}=0.01567 \mu\text{s}$ .

Alternatively, to compensate for photon number fluctuations, it is possible to vary the frequency of the Hadamard pulse rather than its duration. For large step number  $N$ , the photon number distribution is found numerically to approximate

$$P(n) = |\langle n | \rho_w | n \rangle|^2 \sim e^{-\bar{n}} \bar{n}^n / n!, \quad (32)$$

and the width of the photon number distribution  $P(n)$  is closely approximated by

$$\delta n = \sqrt{\langle \hat{n}^2 \rangle - \langle \hat{n} \rangle^2} \approx \sqrt{\bar{n}} \quad (33)$$

in the numerical simulations. Thus, number spreading is negligible, and the walker can be regarded as indeed being concentrated in the locality of one circle in PS [9]. As the walker's initial state is a coherent state with a Poissonian number distribution, the fact that the width remains Poissonian and the amplitude is relatively constant indicates that the initially well-localized walker continues to be localized with respect to amplitude in the phase space over time.

#### IV. LOCALIZATION OF THE WALKER IN PHASE SPACE

We observe from numerical simulations that the walker's location in phase space is effectively localized to a circle in phase space with radial width given by (33). Here we explain why this confinement to the vicinity of a circle in phase space with radius  $\sqrt{\bar{n}}$  is reasonable. This discussion is based on a theoretical analysis of quantum walks on circles in phase space [9].

The evolution of the joint walker+coin system is governed by the effective Hamiltonian (17). There are five terms

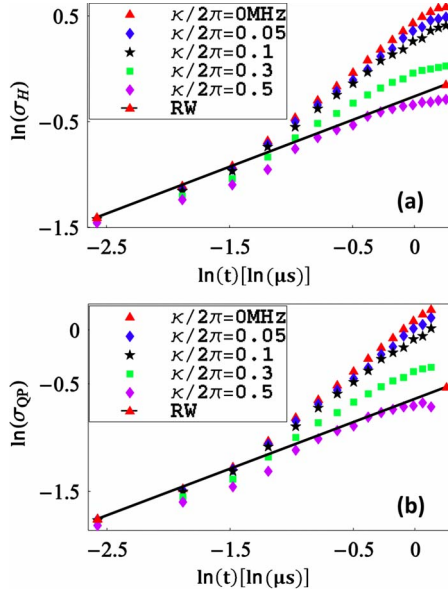


FIG. 3. (Color online) Ln-ln plot of walker spread  $\sigma$  vs  $t$  ( $\mu\text{s}$ ) for (a) a phase distribution on the circle in PS and (b) a QP distribution for different  $\kappa$  and fixed  $(g, \gamma_1, \gamma_\phi)/2\pi = (100, 0.02, 0.31)$  MHz.

on the right-hand side of this Hamiltonian. Let us understand each term and its effect on the dynamics to see why the walker is localized to a circle in phase space.

(i) The first term involves  $\hat{n}\hat{\sigma}_z$ , which is responsible for entangling the evolution of the coin and the walker, effectively to make the walker evolve clockwise or counterclockwise at constant amplitude with the orientation entangled with the state of the coin.

(ii) The second and third terms involve the operators  $\hat{\sigma}_z$  and  $\hat{n}$ , respectively, which correspond to energies, hence frequencies, for the coin and walker.

(iii) The fourth term, involving  $\hat{\sigma}_x$ , is responsible for the Hadamard coin flip and is proportional to the Rabi frequency, which is itself proportional to the pulsed driving field  $\epsilon$ , Eq. (19).

(iv) The fifth term is a displacement involving the operator  $\hat{a} + \hat{a}^\dagger$ , which pushes the walker off the circle, and is proportional to  $\epsilon$ .

In making the quantum walk work, the goal is to make the Rabi frequency  $\Omega_R$  large, but keep  $\epsilon$  small in order to flip the coin, but minimally shift the walker from the circle.

We have been able to simultaneously achieve the two conditions of large Rabi frequency and small displacement. By

meeting these two conditions, the evolution is closely approximated by the unitary evolution

$$H \otimes D(i\lambda/\sqrt{2}) \quad (34)$$

for the quantum walk on circles in phase space [9], with  $\lambda = \sqrt{2}\epsilon t_H$  the size of the displacements from the circle. The resultant photon number spread after  $N$  steps is [9]

$$\delta n \approx \sqrt{\frac{\sqrt{\bar{n}_0}(1 + \cos \Delta\theta)}{2}} + \frac{\lambda \left[ 2 + \cos \Delta\theta - \cos N\Delta\theta + \frac{\cos(1-N)\Delta\theta}{\sin^2 \Delta\theta/2} \right]}{2\sqrt{2}\sqrt{1 + \cos \Delta\theta}}. \quad (35)$$

For large  $\bar{n}_0$  and small  $\lambda$ ,  $\delta n \sim \sqrt{\bar{n}}$ . Hence, in the asymptotic large-mean-photon-number  $\bar{n}$  limit, the reduced walker state has support almost entirely from coherent states with amplitude  $\sqrt{\bar{n}}$ . This means that the joint state of the walker+coin can be regarded approximately as an entanglement of a walker in superpositions of coherent states with the coin state. This approximation guarantees that the walker can be regarded as being localized to one circle in phase space with a Poissonian spread in photon number that does not increase significantly over time provided that the phase steps are small and  $\bar{n}$  is large.

## V. OPEN SYSTEM AND MEASUREMENT

Coupling to additional uncontrollable degrees of freedom leads to energy relaxation and dephasing in the system. In the Born-Markov approximation, these effects can be characterized by a resonator photon leakage rate  $\kappa$  (determined at fabrication time by the resonator input and output coupling capacitances), an energy relaxation rate  $\gamma_1$ , and a pure dephasing rate  $\gamma_\phi$  for the qubit. The open system thus evolves according to

$$\dot{\rho} = -i[\hat{H}_{\text{eff}}, \rho] + \kappa\mathcal{D}[\hat{a}]\rho + \gamma_1\mathcal{D}[\hat{\sigma}_-]\rho + (\gamma_\phi/2)\mathcal{D}[\hat{\sigma}_z]\rho, \quad (36)$$

with

$$\mathcal{D}[\hat{L}]\rho \equiv (2\hat{L}\rho\hat{L}^\dagger - \hat{L}^\dagger\hat{L}\rho - \rho\hat{L}^\dagger\hat{L})/2. \quad (37)$$

TABLE I. The linear regression data  $\ln \sigma_H = (s \pm \Delta s) \ln t + (\ln \sigma_H^0 \pm \Delta \ln \sigma_H^0)$  of the Holevo standard deviation of phase distribution on a Ln-ln scale for lossy cavities.

$\kappa/2\pi(\text{MHz})$	$s$	$\Delta s$	$\ln \sigma_H^0$	$\Delta \ln \sigma_H^0$	$r$
0	0.924	0.009	0.442	0.004	0.990
0.05	0.879	0.013	0.362	0.006	0.991
0.1	0.822	0.014	0.279	0.008	0.992
0.3	0.615	0.022	-0.025	0.012	0.993
0.5	0.447	0.030	-0.309	0.017	0.990

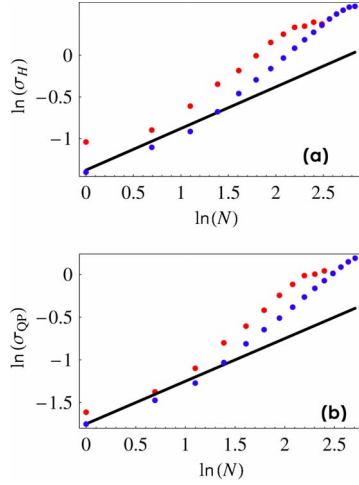


FIG. 4. (Color online) Ln-ln plot of walker's phase spread  $\sigma$  vs  $N$  (the number of the steps) to  $N=15$  with fixed pulse duration  $0.0157 \mu\text{s}$  for (a) a phase distribution on the circle in PS and (b) a QP distribution for the classical random walk (solid line) and the QW (red dots) with  $\alpha=3$ ,  $d=21$ , and typical system parameters  $(\omega_a, \omega_r, g, \epsilon)/2\pi = (7000, 5000, 100, 1000)$  MHz. In comparison, the blue dotted lines are for the QW with adaptive pulse durations, which break down after 15 steps.

Relaxation and dephasing of a charge qubit in circuit QED were reported in [11] as  $T_1=7.3 \mu\text{s}$  and  $T_2=500 \text{ ns}$ . These translate to

$$\gamma_1/2\pi = 0.02 \text{ MHz} \quad (38)$$

and

$$\gamma_\phi/2\pi = (\gamma_2 - \gamma_1/2)/2\pi = 0.31 \text{ MHz}. \quad (39)$$

The master equation (36) is used to compute  $\rho(t)$  from which the reduced state of the walker  $\rho_w$  is obtained and thence the phase distribution  $P_w(\theta)$ , Eq. (3). Empirically the phase distribution can be obtained by performing full optical homodyne tomography on the transmission line resonator to obtain  $W(x, p)$  [17] from which  $P_w(\theta)$  can be computed and  $\sigma_H(t)$  thereby determined. The scaling of  $\sigma_H$  with  $t$  in Eq. (13) is a convenient empirical signature of the RW vs the QW.

As full tomography is expensive, it would be valuable to observe a QW directly from optical homodyne detection with a single choice of local oscillator phase  $\varphi$  instead of having to scan over many  $\varphi$  for full tomography. Our simulations

show both  $\sigma_H(t)$  for  $P_w(\theta)$  and  $\sigma_{QP}$  for the QP distribution at  $\varphi=0$ , with the choice of  $\varphi=0$  corresponding to having a local oscillator that is in phase with the walker at  $t=0$ . For our choices of realistic experimental parameters, the walker's phase distribution spreads from  $-\pi$  to  $\pi$  on a scale of 15 steps, so simulations are limited to fewer than 15 steps before the spreading effectively saturates and our comparison of the QW vs the RW breaks down.

Simulated evolutions of  $\sigma_H(t)$  and  $\sigma_{QP}(t)$  are presented in Figs. 3(a) and 3(b), respectively. Corresponding linear regression data presented in Tables I and II clearly reveals slopes compatible with the characteristic quadratic decrease in phase spreading for increasing decoherence of the QW until the transition to the RW [4].

These results show the significance of  $\kappa$  in decoherence from the QW to the RW. Moreover,  $\kappa$  is much more important than  $\gamma_1$  and  $\gamma_\phi$  with respect to the scaling of  $\sigma_{H,QP}$  with  $t$ . The pure dephasing rate  $\gamma_\phi$  mainly leads to smearing of the phase distribution and the phase distribution loses its symmetry. Furthermore, the effect of the energy relaxation rate  $\gamma_1$  is small here compared with  $\kappa$  because of our realistic choice of parameters.

Unfortunately  $\kappa$  must be low to obtain a QW, yet high to allow fast readout. This dilemma is resolved by instead using two modes [18]: one resonator (labeled  $a$ ) of high  $Q$  and acting as the walker and a second resonator (labeled  $b$ ) of low  $Q$  and used for fast readout [12]. The microwave radiation from resonator  $a$  is coupled into resonator  $b$ , and measurements ensue on resonator  $b$ . Measurements must be quick on the time scale of the walker's steps, so it cannot be longer than the time scale between pairs of Hadamard pulses. In the two-resonator system,  $\kappa_b$  has therefore a lower bound of  $O(g^2/\Delta)$ .

Due to coupling to resonator  $b$ , the transition frequency of the CPB in resonator  $a$  and the pure dephasing rate are changing with the cavity field in resonator  $b$ , so the master equation for resonator  $a$  and the CPB is modified to [12]

$$\dot{\rho} = -i[\hat{H}_s, \rho] + \kappa_a \mathcal{D}[\hat{a}]\rho + \gamma_1 \mathcal{D}[\hat{\sigma}_-]\rho + \frac{\gamma_\varphi + \Gamma_m}{2} \mathcal{D}[\hat{\sigma}_z]\rho, \quad (40)$$

with

$$\hat{H}_s = \omega_{rb} \hat{n} + \frac{\Omega'(t)}{2} \hat{\sigma}_z + [g \hat{a}^\dagger \hat{\sigma}_- + \epsilon(t) \hat{a}^\dagger e^{-i\omega_d t} + \text{H.c.}], \quad (41)$$

where

TABLE II. The linear regression data  $\ln \sigma_{QP} = (s \pm \Delta s) \ln t + (\ln \sigma_{QP}^0 \pm \Delta \ln \sigma_{QP}^0)$  of the standard deviation of QP distribution on a ln-ln scale for lossy cavities.

$\kappa/2\pi(\text{MHz})$	$s$	$\Delta s$	$\ln \sigma_{QP}^0$	$\Delta \ln \sigma_{QP}^0$	$r$
0	0.937	0.006	0.093	0.004	0.988
0.05	0.892	0.009	0.016	0.006	0.989
0.1	0.832	0.013	-0.068	0.008	0.990
0.3	0.634	0.020	-0.372	0.012	0.993
0.5	0.453	0.034	-0.677	0.019	0.990

$$\Omega'(t) = \omega_a + 2\chi_b[|\alpha_b(t)|^2 + 1/2] \quad (42)$$

and

$$\Gamma_m = 8\chi_b^2|\alpha_b(t)|^2/\kappa_b. \quad (43)$$

In these expressions,  $\chi_b = g_b^2/(\omega_a - \omega_{rb})$  is the cavity pull of the measurement resonator  $b$  and  $\alpha_b(t)$  is the classical part of the measurement cavity field. Under these conditions, the master equation for the CPB and resonator  $b$ , Eq. (40), is identical to Eq. (36) except for a parameter change. It is interesting to note that, in this two-resonator case, qubit dephasing can be tuned by changing the number of photons injected in the readout resonator (corresponding to measurement-induced dephasing [10]). As a result, it should be possible to observe the crossover between the QW and the RW as a function of this tunable dephasing.

In summary, we have introduced the following protocol to implement the QW on circles in PS using circuit QED. (i) Solve the Schrödinger equation from  $t=0$  to  $t=N(t_H^{(0)} + \tau)$ , to obtain the mean photon number  $\bar{n}(t)$  from which the sequence  $\{\bar{n}_j\}$  and  $\{t_H^{(j)}\}$  are obtained. (ii) Prepare a high- $Q$  resonator in its vacuum state (by simply cooling). (iii) When the vacuum state is prepared, inject a microwave field with a Gaussian pulse shape and temporal width  $T_G$  in order to prepare the high- $Q$  resonator in a coherent state  $|\alpha\rangle$ . (iv) After  $t=2T_G$ , implement the Hadamard pulse on the CPB by injecting a square pulse of frequency  $\omega_d$  into resonator  $b$  over time scale  $t_H^{(j)}$  for step  $j$ . (v) Terminate the external driving of the resonator to allow free evolution over time scale  $\tau$ . (vi) Repeat steps (iv) and (v)  $N$  times. (vii) Perform full tomography on resonator  $b$  by performing homodyne measurement over many values of  $\phi$  and use standard inversion technique on the data.

In circuit QED, the amplifier thermal noise is significant, with more thermal photons present than the mean resonator photon number [11]. However, the signal QP distribution and full Wigner function can be obtained from the resultant homodyne detection statistics by convolving the readout with a thermal function (which is a Gaussian mixture of Gaussian states centered at the PS origin). The spread of the convolution is determined by the mean thermal photon number, which is typically 20.

The result is expected to be noisy quadrature phase readout, but repetition will yield, on average, the desired linearity of  $\ln \sigma$  vs  $\ln t$ . We can use a filter algorithm [19] which takes the inversion formula for the measured Radon transform of the Wigner function with thermal noise and reconstruct the Wigner function of the corresponding noiseless signal. Hence we can achieve the noiseless phase distribution and QP distribution with the Wigner function of the noiseless signal.

## VI. CONCLUSIONS

We have shown that the QW on circles in PS can be implemented via circuit QED with and without open-system effects using realistic parameters and find that the signature of the QW is evident under those conditions. Moreover, full

tomography may not be required because direct homodyne measurements over few quadratures reveal an unambiguous QW signature, and the RW can controllably emerge by tuning decoherence. Our scheme shows how a QW with just one walker can be implemented in a realistic system, and controllable decoherence can be performed, thereby allowing continuous tunability between the quantum and classical regimes.

Our scheme allows only a finite number of steps before the quadratic enhancement in phase spreading breaks down. As the phase step  $\Delta\theta$  must be strictly greater than  $1/\delta n$ , the number of steps,  $N$ , has an upper bound because of the desire to avoid wraparound effects (the walker going around the circle); then,  $N < 2\pi/\Delta\theta$ . Therefore,  $N < 2\pi\delta n \approx 2\pi\sqrt{\bar{n}}$  provides an upper bound on  $N$ .

Hence the number of steps has an upper bound that is determined by  $\bar{n}$ . If the mean number of photons in the resonator is increased, so is the allowed number of steps. Physically, however, the mean number of photons cannot be too large because the dispersive approximation that we exploit fails for large cavity photon number: this breakdown occurs for critical photon number [10,20]

$$\bar{n}_{\text{crit}} = \frac{\Delta^2}{4g^2}. \quad (44)$$

Equation (44) yields an upper bound of photon number in the resonator and limits the number of steps the walker can take and exhibits a quadratic enhancement of spreading. In our example,  $\Delta=2000$  MHz and  $g/2\pi=100$  MHz, so  $\bar{n}_{\text{crit}}=100$ . Here we have treated the case of just nine photons and seen strong evidence of a quadratic enhancement of phase diffusion, so the quantum quincunx effectively works well below this critical photon number where the dispersive approximation breaks down.

In our scheme, the pulse duration  $t_H$  is adjusted each time according to the predicted mean photon number, but precise control of the Hadamard pulse may be difficult to achieve in experiments.

In Fig. 4 we have shown a simulation of the cases with and without adjusting the duration of the Hadamard pulse sequence. Not adjusting the Hadamard pulse durations still yields a quadratic enhancement of the phase distribution due to the quantum walk, but it breaks down earlier. In our simulation, the breakdown occurs after 10 steps rather than 15 for the adaptive pulse duration. For the first 10 steps, the numerically simulated standard deviation for the QP distribution and the Holevo standard deviation on  $\ln$ - $\ln$  scale are, respectively, shown to be approximately linear in  $\ln N$ :  $\ln \sigma_{\text{QP}} = (0.939 \pm 0.007)\ln N + (-2.090 \pm 0.005)$ , the  $r$  coefficient being 0.99, and  $\ln \sigma_{\text{H}} = (0.890 \pm 0.006)\ln N + (-1.563 \pm 0.003)$ , the  $r$  coefficient being 0.96.

## ACKNOWLEDGMENTS

This work has been supported by NSERC, MITACS, CIFAR, FQRNT, QuantumWorks, and iCORE. We thank Stephen Bartlett, Jay Gambetta, Steve Girvin, and Rob Schoelkopf for helpful discussions.

- [1] D. Aharonov, A. Ambainis, J. Kempe, and U. Vazirani, in *Proceedings of the 33rd ACM Symposium on the Theory of Computing* (ACM, Washington, DC, 2001), p. 50.
- [2] A. M. Childs, R. Cleve, E. Deotto, E. Farhi, S. Gutmann and D. A. Spielman, in *Proceedings of the 35th ACM Symposium on the Theory of Computing* (ACM, Washington, DC, 2003), p. 59.
- [3] B. C. Travaglione and G. J. Milburn, *Phys. Rev. A* **65**, 032310 (2002).
- [4] B. C. Sanders, S. D. Bartlett, B. Tregenna, and P. L. Knight, *Phys. Rev. A* **67**, 042305 (2003).
- [5] T. Di, M. Hillery, and M. S. Zubairy, *Phys. Rev. A* **70**, 032304 (2004).
- [6] D. Bouwmeester, I. Marzoli, G. P. Karman, W. Schleich, and J. P. Woerdman, *Phys. Rev. A* **61**, 013410 (1999).
- [7] V. Kendon and B. C. Sanders, *Phys. Rev. A* **71**, 022307 (2005).
- [8] E. T. Jaynes and F. W. Cummings, *Proc. IEEE* **51**, 89 (1963).
- [9] P. Xue and B. C. Sanders, *New J. Phys.* **10**, 053025 (2008).
- [10] A. Blais, R. S. Huang, A. Wallraff, S. M. Girvin, and R. J. Schoelkopf, *Phys. Rev. A* **69**, 062320 (2004).
- [11] A. Wallraff, D. I. Schuster, A. Blais, L. Frunzio, J. Majer, M. H. Devoret, S. M. Girvin, and R. J. Schoelkopf, *Phys. Rev. Lett.* **95**, 060501 (2005); A. Wallraff, D. I. Schuster, A. Blais, L. Frunzio, R.-S. Huang, J. Majer, S. Kumar, S. M. Girvin, and R. J. Schoelkopf, *Nature (London)* **431**, 162 (2004); D. I. Schuster, A. Wallraff, A. Blais, L. Frunzio, R.-S. Huang, J. Majer, S. M. Girvin, and R. J. Schoelkopf, *Phys. Rev. Lett.* **94**, 123602 (2005).
- [12] R. J. Schoelkopf, J. M. Gambetta *et al.* (private communication).
- [13] A. S. Holevo, *Lect. Notes Math.* **1055**, 153 (1984).
- [14] H. M. Wiseman and R. B. Killip, *Phys. Rev. A* **56**, 944 (1997).
- [15] D. I. Schuster, A. A. Houck, J. A. Schreier, A. Wallraff, J. M. Gambetta, A. Blais, L. Frunzio, J. Majer, B. Johnson, M. H. Devoret, S. M. Girvin, and R. J. Schoelkopf, *Nature (London)* **445**, 515 (2007).
- [16] A. Blais, J. Gambetta, A. Wallraff, D. I. Schuster, S. M. Girvin, M. H. Devoret, and R. J. Schoelkopf, *Phys. Rev. A* **75**, 032329 (2007).
- [17] K. Vogel and H. Risken, *Phys. Rev. A* **40**, 2847 (1989).
- [18] H. M. Wiseman and G. J. Milburn, *Phys. Rev. A* **47**, 642 (1993).
- [19] S. Chountasis, L. K. Stergioulas, and A. Vourdas, *J. Mod. Opt.* **46**, 2131 (1999).
- [20] M. Boissonneault, J. Gambetta, and A. Blais, *Phys. Rev. A* **77**, 060305 (2008).